Conference Paper, Published Version

Karambas, Theofanis; Makris, Christos; Baltikas, Vassileios

2-DH Post-Boussinesq Modeling of Nonlinear Wave Propagation and Transformation in Nearshore Zones and Inside Ports

Coastal Structures 2019 - Nils Goseberg, Torsten Schlurmann (eds) - © 2019 Bundesanstalt für Wasserbau
ISBN 978-3-939230-64-9 (Online) - DOI: 10.18451/978-3-939230-64-9_074

2-DH Post-Boussinesq Modeling of Nonlinear Wave Propagation and Transformation in Nearshore Zones and Inside Ports

Th. V. Karambas, C. V. Makris & V. N. Baltikas
School of Civil Engineering, Aristotle University of Thessaloniki, 54124, Thessaloniki, Greece

Abstract: An updated version of a 2-DH post-Boussinesq wave model is introduced. The model is wavenumber free and as far as the linear dispersion relation is concerned, the approach is exact. It is implemented for the wave propagation and transformation due to shoaling, refraction, diffraction, bottom friction, wave breaking, wave-structure interaction, reflection, wave-current interaction, etc. in nearshore zones and specifically inside ports and in the vicinity of coastal structures. Thorough validation of the model is attempted by comparisons with output from classic laboratory-scale wave flume experiments as well as analytical solutions. Physical cases of both regular and irregular wave fields are numerically reproduced with acceptable accuracy. Results concerning a case study in a characteristic Greek port setup are also presented and seem encouraging for realistic scale simulations.

Keywords: wave modeling, post-Boussinesq model, wave propagation, wave transformation, nearshore, ports, non-linear waves, irregular waves

1 Introduction

The propagation of non-linear dispersive waves in shallow waters is traditionally numerically modelled by the classic Boussinesq-type equations (Peregrine, 1967). However, for the early versions of Boussinesq-type models there are still application constraints concerning restrictions of simulations to non-breaking waves in water depths $d<0.2L$ (L is the local wave length). The work of Madsen et al. (1991) extended the applicability of the Boussinesq-type models by incorporating linear dispersion for deeper waters with extension of the relevant equations. During the 90's, many researchers have produced new versions of Boussinesq-type models within the coastal engineering/science community (Karambas and Koutitas, 1992; Nwogu, 1993; Wei and Kirby, 1995; Wei et al., 1995; Madsen and Schäffer, 1998; Karambas, 1999; Zou, 1999; etc.). These endeavors mainly account for fundamental improvements of dispersive properties for wave frequency and addition of wave breaking dissipation mechanisms (surface roller and eddy viscosity models). The latter ameliorations allowed Boussinesq-type models to be widely implemented by coastal engineers for nearshore flow simulations. Further advanced versions of these models by the coastal research community established the Boussinesq-type approaches as the main modelling tool by practitioners in coastal and port engineering. In this framework, Brocchini (2013) presents a comprehensive review and the reasons behind the prevalence of Boussinesq-type models, based on their ability to blend the modeling robustness with computational efficiency by modern hardware resources.

1.1 Recent developments

More recent developments during the last 20 years practically eradicate application restrictions due to the water depth (waves with $kd\leq25$; $k=2\pi/L$ the wavenumber) and allow for good accuracy (dispersion factor up to $kd\approx12$) in simulations of highly nonlinear waves (Madsen et al., 2002; 2003; Bingham and Agnon, 2005). However, solvability issues of the newly produced Boussinesq-type equations still

remained, referring to stability and accuracy of the proposed integration schemes for solving complex systems of partial differential equations (PDEs) with a large number of high-order derivative terms. Tsutsui et al. (1998) derived a system of fully dispersive weakly non-linear equations in terms of the surface elevation and the depth-averaged horizontal velocity, replacing phase celerity terms in the momentum equations by integral forms with the use of a kernel of Fourier-transformed phase velocity. Hence, similarly proposed models became wavenumber free, and allow for description of irregular wave propagation over any finite water depth. New versions of a post-Boussinesq type of wave model were proposed by Schäffer (2003, 2004) treating nonlinear fully dispersive waves, in terms of free-surface elevation and horizontal particle velocities at still water level. Convolution integrals in space were introduced, with the use of appropriate impulse functions, in order to handle internal kinematics of the hydrodynamic field in the water column.

1.2 Scope of paper

Karambas and Memos (2009) presented a similar post-Boussinesq type of model, proposing a system of 2-DH equations for fully dispersive and weakly nonlinear irregular waves over any finite water depth. Five terms were introduced in each momentum equation, including terms for long wave propagation and frequency dispersion in the numerical solution. Solution was based on an explicit Finite Differences (FD) scheme and an estimation of the aforementioned convolution integral, restricting the system of algebraic equations compared to other Boussinesq-type model formulations. In this work, an updated version of the 2-DH post-Boussinesq wave model of Karambas and Memos (2009) is introduced. It is implemented for the wave propagation and transformation (due to shoaling, refraction, diffraction, bottom friction, wave breaking, wave-structure interaction, reflection, wave-current interaction, etc.) at nearshore zones in the vicinity of coastal structures and specifically inside ports. One of the main goals of the paper is the model's thorough validation. Regarding its capabilities in representing the propagation of regular and irregular non-linear waves, the model was tested against the analytical solution of Helmholtz equation for wave diffraction, as well as versus experimental data for monochromatic and spectral wave propagation over complex bathymetries and sloping topographies (Berkhoff et al., 1982; Vincent and Briggs, 1989). The model was furthermore validated by comparisons with experimental data for uni- and multi-directional spectral wave diffraction through a breakwater gap (Li et al., 2000; Yu et al., 2000). A case study of model application over a realistic bathymetry in areas around and inside a characteristic Greek port is also presented.

2 Model description and numerical scheme

The proposed post-Boussinesq wave model is thus wavenumber free and, as far as the linear dispersion relation is concerned, the approach is exact (*i.e.* the model poses no restriction on water depth). Wave breaking is further incorporated in the model by adopting the surface roller concept (Schäffer et al., 1993).

2.1 Model equations

Karambas and Memos (2009) analytically describe the theoretical formulation of the proposed model, which is valid for irregular, fully dispersive, weakly nonlinear waves in an inviscid and incompressible fluid propagating over mildly sloping bottoms. For the 2-DH version, the momentum equations are written:

$$\frac{\partial U}{\partial t}+U\frac{\partial U}{\partial x}+V\frac{\partial U}{\partial y}+g\frac{\partial \zeta}{\partial x}=-\int_{\infty}^{\infty}\int_{-\infty}^{\infty}\left(\frac{\partial \zeta}{\partial x}(x-\xi_1,x-\xi_2,t)-\frac{\partial \zeta}{\partial x}\right)K(\xi_1,\xi_2)\,d\xi_1 d\xi_2 \tag{1}$$

$$\frac{\partial V}{\partial t}+U\frac{\partial V}{\partial x}+V\frac{\partial V}{\partial y}+g\frac{\partial \zeta}{\partial y}=-\int_{-\infty}^{\infty}\int_{-\infty}^{\infty}\left(\frac{\partial \zeta}{\partial y}(x-\xi_1,x-\xi_2,t)-\frac{\partial \zeta}{\partial y}\right)K(\xi_1,\xi_2)\,d\xi_1 d\xi_2 \tag{2}$$

where t is the time, U and V are the depth-averaged velocity in x- and y-direction, respectively, ζ is the free surface elevation, ξ_1 and ξ_2 are the conjugate variable terms of the Fourier transform, and the kernel $K(x,y)$ is given by:

$$K(x,y)=\frac{g}{2\pi d^2}\left[\frac{1}{r/d}-\sum_{n=1}^{\infty}\frac{(-1)^{n-1}}{\sqrt{n^2+(r/d)^2/4}}\right] \tag{3}$$

with $r^2=x^2+y^2$. The momentum Eqs. (1 and 2) together with the continuity Eq. (4) constitute the system of model equations for the 2-DH case:

$$\frac{\partial\zeta}{\partial t}+\frac{\partial\left((d+\zeta)U\right)}{\partial x}+\frac{\partial\left((d+\zeta)V\right)}{\partial y}=0 \tag{4}$$

Wave energy dissipation due to depth-limited wave breaking in the present model is primarily based on the "surface roller" approach. Wave attenuation due to the roller is introduced as an excess momentum term due to non-uniform vertical velocity distribution (Schäffer et al., 1993), while the surface roller is transported by wave celerity c = (c_x,c_y):

$$\begin{aligned} &u=c_x \ , v=c_y \quad \text{for} \quad \zeta-\delta\le z\le\zeta \\ &u=u_o \ , \ v=v_o \quad \text{for} \quad -d\le z\le\zeta-\delta \end{aligned} \tag{5}$$

where c_x and c_y = wave celerity components, δ is the thickness of the roller, and u_o, v_o = core velocities, both pairs in x-and y- directions. Thus, Eq. (1 and 2) become:

$$\frac{\partial U}{\partial t}+\frac{U\partial U}{\partial x}+\frac{V\partial U}{\partial y}+g\frac{\partial\zeta}{\partial x}+\frac{1}{d+\zeta}\left(\frac{\partial R_{xx}}{\partial x}+\frac{\partial R_{xy}}{\partial y}\right)=-\int_{\infty}^{\infty}\int_{-\infty}^{\infty}\left(\frac{\partial\zeta}{\partial x}(x-\xi_1,x-\xi_2,t)-\frac{\partial\zeta}{\partial x}\right)K(\xi_1,\xi_2)\,d\xi_1 d\xi_2 \tag{6}$$

$$\frac{\partial V}{\partial t}+\frac{U\partial V}{\partial x}+\frac{V\partial V}{\partial y}+g\frac{\partial\zeta}{\partial y}+\frac{1}{d+\zeta}\left(\frac{\partial R_{yy}}{\partial y}+\frac{\partial R_{xy}}{\partial x}\right)=-\int_{-\infty}^{\infty}\int_{-\infty}^{\infty}\left(\frac{\partial\zeta}{\partial y}(x-\xi_1,x-\xi_2,t)-\frac{\partial\zeta}{\partial y}\right)K(\xi_1,\xi_2)\,d\xi_1 d\xi_2 \tag{7}$$

$$\begin{aligned} R_{xx}&=\frac{\delta}{1-\delta/(d+\zeta)}\left(c_x-U\right)^2 \\ R_{yy}&=\frac{\delta}{1-\delta/(d+\zeta)}\left(c_y-V\right)^2 \\ R_{xy}&=\frac{\delta}{1-\delta/(d+\zeta)}\left(c_x-U\right)\left(c_y-V\right) \end{aligned} \tag{8}$$

By checking if the local slope of the free-surface elevation exceeds an initial critical value, we can control the incipient wave breaking. Roller region and thickness δ are determined geometrically (Sørensen et al., 1998).

2.2 Numerical scheme

The numerical solution is accomplished by a widely used simple and well-documented explicit 2nd order FD scheme centered in space and forward in time on a staggered grid (Karambas and Memos, 2009), conserving mass and energy for non-breaking waves in a satisfactory manner. The discrete continuity equation is centered in the level points and the momentum equations in the flux points.

The partial differential equations Eq. (1, 2 and 4) are approximated by the following algebraic FD equations according to the selected explicit scheme (Koutitas, 1988):

$$\frac{\zeta_i^{n+1}-\zeta_i^{n}}{\Delta t}+\frac{(U\overline{(d+\zeta)})_{i+1,j}^{n}-(U\overline{(d+\zeta)})_{i,j}^{n}}{\Delta x}+\frac{(V\overline{(d+\zeta)})_{i,j+1}^{n}-(V\overline{(d+\zeta)})_{i,j}^{n}}{\Delta y}=0 \tag{9}$$

$$\frac{U_{i,j}^{n+1}-U_{i,j}^{n}}{\Delta t}+U_{i,j}^{n}\frac{U_{i+1,j}^{n}-U_{i-1,j}^{n}}{2\Delta x}+\bar{V}_{i,j}^{n}\frac{U_{i,j+1}^{n}-U_{i,j-1}^{n}}{2\Delta y}+g\frac{\zeta_{i,j}^{n+1}-\zeta_{i-1,j}^{n+1}}{\Delta x}=I^{n+1} \tag{10}$$

$$\frac{V_{i,j}^{n+1}-V_{i,j}^{n}}{\Delta t}+\bar{U}_{i,j}^{n}\frac{V_{i+1,j}^{n}-V_{i-1,j}^{n}}{2\Delta x}+V_{i,j}^{n}\frac{V_{i,j+1}^{n}-V_{i,j-1}^{n}}{2\Delta y}+g\frac{\zeta_{i,j}^{n+1}-\zeta_{i,j-1}^{n+1}}{\Delta y}=I^{n+1} \tag{11}$$

where I is the convolution integral term, Δt and Δx, Δy are the time and space discretisation steps, respectively, i and j are the number of center grid cells in x- and y-axis, respectively, n is the number of center time step, and the overbar denotes a mean value according to Karambas and Memos (2009).

The convolution integrals of Eq. (6 and 7) are calculated numerically by higher order accurate methods (extended Simpson's or Newton's 3/8 rules). The horizontal radius of the kernel in the convolution integrals, which are in turn based on impulse response functions displaying exponential decay, are taken as $\pm 4d$ (*i.e.* approximately four times the local water depth), instead of $\pm\infty$, in order to limit the computational times of integration. Decomposition rates of kernel values with normalized distance x/d away from any arbitrary grid cell of integration for the bell-shaped function are given in Karambas and Memos (2009) and Schäffer (2004). The relevant summation terms in Eq. (3) change +/– sign and therefore follow a slow convergence. Acceleration of the latter is achieved by means of an Euler's transformation approach (Press et al., 1986), restricting the addition to no more than 25 terms. This way we can significantly increase the computational speed of the model.

The presence of vertical structures is incorporated by introducing a total reflection boundary condition ($U = 0$ or $V = 0$). Partial reflection is also simulated, by introducing an artificial eddy viscosity coefficient ν_h. The values of ν_h are estimated from the method developed by Karambas and Bowers (1996) for given values of the reflection coefficient from literature.

2.3 Internal wave generation and sponge layer technique

In the present model, the waves are generated along a generation line parallel to the offshore boundary by applying the source term addition method. In this method the values η_i^* of surface elevation are added to the corresponding surface elevation values that are computed by the model and given by (Larsen, and Dancy, 1983; Lee and Suh, 1998):

$$\eta_i^* = 2\eta^I \cos\theta \; c\frac{dt}{dx}, \qquad \eta^I = \frac{H_i}{2}\sin\left(kx+ky-\omega t\right) \tag{12}$$

where, H_i is the incident wave height, $k = 2\pi/L$, ω is the angular frequency ($\omega = 2\pi/T$, T is the wave period), θ is the wave propagation angle with respect to the x- or y-axis, c is the wave celerity, dx is the typical grid cell size and dt is the time step of numerical solution.

The model is also able to simulate irregular uni- and multi-directional waves. The generation and propagation of spectral waves may furthermore account for several different angles and directions simultaneously. Following the modeling approach of Miles (1989) and Lee and Suh (1998), the incident surface elevation function is given by:

$$\eta^I(x,y,t)=\sum_{n=1}^{N}\sum_{m=1}^{M}A_{nm}\cos\left(k_{nm}x\cos\theta_m+k_{nm}y\sin\theta_m-\omega_{nm}t+\varepsilon_{nm}\right) \tag{13}$$

where N and M are the numbers of frequency bands and directional bands in the discretized directional spectrum, $A_{nm}=\sqrt{2\,S(f_{nm})\,D(f_{nm},\theta_m)M\,df\,d\theta}$ is the wave amplitude, $S(f_{nm})$ is the frequency spectrum, ω_{nm} is the wave angular frequency, df is the frequency interval, θ_m is the wave propagation angle, $d\theta$ is the wave propagation angle interval and ε_{nm} is the random phase.

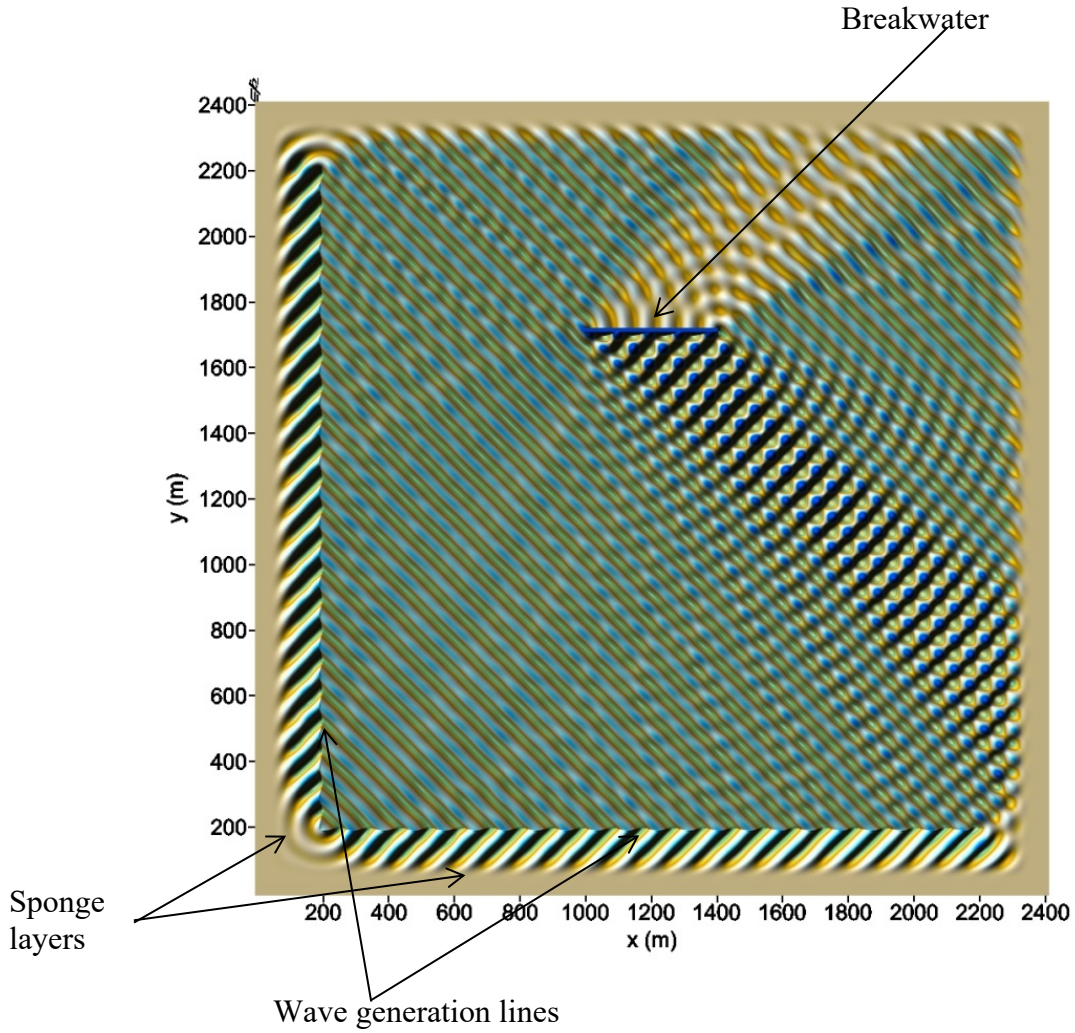

Fig. 1. Snapshot of free-surface elevation of oblique incident regular waves: generation, absorption and reflection by a breakwater.

The directional spreading function $D(f,\theta)$, based on a Fourier series representation for the wrapped normal spreading function, is written (see also Vincent and Briggs, 1989):

$$D(f,\theta) = \frac{1}{2\pi} + \frac{1}{\pi}\sum_{k=1}^{K} \exp\left[-\left(\frac{k\sigma_m}{2}\right)\right] cos[k(\theta - \bar{\theta})] \tag{14}$$

where F is the max number of k_f terms in the series, $\overline{\theta}$ the mean wave direction and σ_m is the directional spreading parameter.

In order to avoid diffraction problems, in the case of oblique incidence, the waves are generated simultaneously in two lines parallel to x- and y-axis, in the lower and lateral boundaries. Sponge layers are placed at the outer open boundaries to dissipate wave energy inside them and thus minimize wave reflection from the boundaries (Larsen and Dancy, 1983). According to this technique, the sponge layer gradually absorbs the wave energy by multiplying ζ, U and V with the energy dissipation rate ν, calculated by the improved scheme proposed by Yoon and Choi (2001), given as follows:

$$\begin{aligned} &\nu(x_*) = \exp\left[-(b^{x_*/\Delta x} - b^{x_S/\Delta x})\ln\Lambda\right], \quad 0 \le x_* \le x_S \\ &\nu(x_*) = 1, \qquad\qquad\qquad\qquad x_* > x_S \\ &b = \left[1 + r_s + \exp(-1/r_s)\right], \quad r_s = 10/t_s \end{aligned} \tag{15}$$

where x_s is the width of the sponge layer, x_* is the location in the sponge layer, t_s the number of grid points inside the sponge layer, and the parameter Λ is set as 2.

Fig. 1 shows the instantaneous free-surface elevation of oblique regular waves propagating in the computational domain (H_i = 1.0 m, $\theta = 45^o$, T = 8 sec).

3 Model validation

Evaluation of the model's performance is conducted by comparisons of simulation results with experimental data of regular and irregular wave diffraction around semi-infinite breakwaters and through breakwater gaps (Yu et al. 2000; Li et al. 2000). The elliptical shoal experimental setup by Vincent and Briggs (1989) with a directional spectral wave generator is also numerically reproduced as a test.

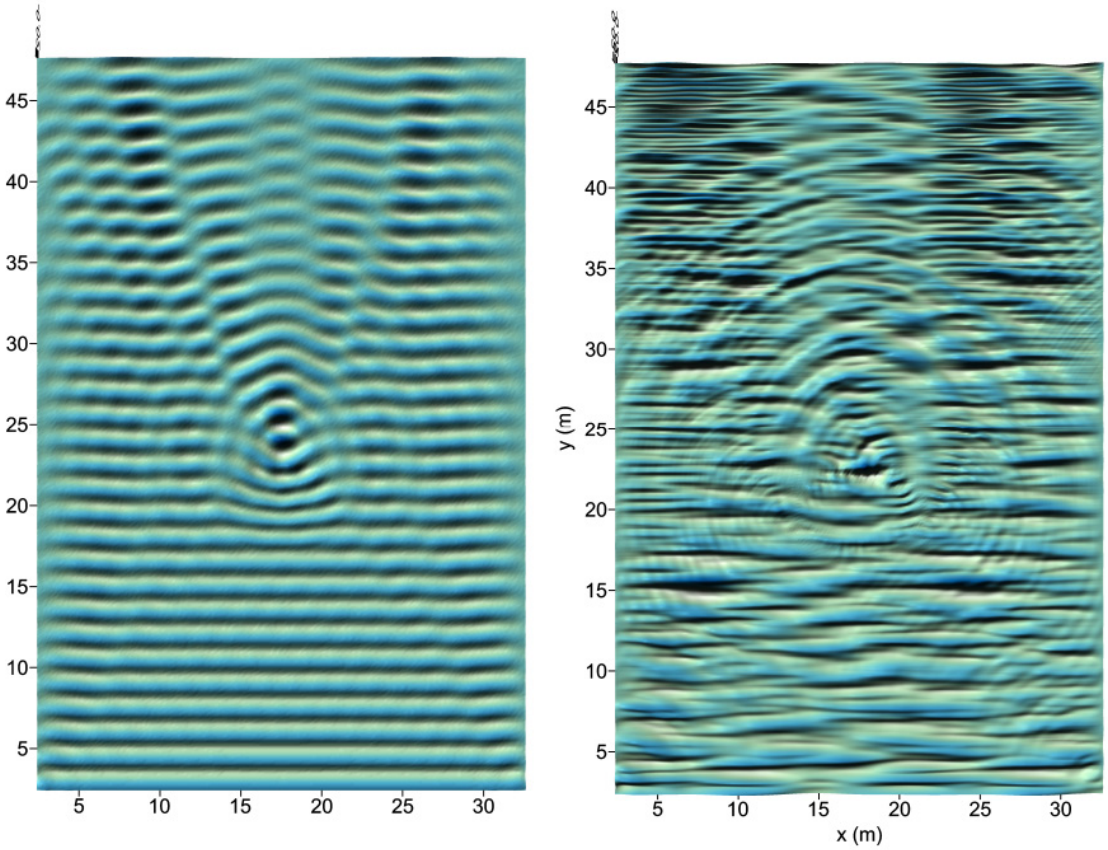

Fig. 2. Monochromatic and multi-directional wave propagation over a shoal: snapshot of free-surface elevation.

3.1 Irregular wave propagation over elliptical shoal

The shoal experiments were reported by Vincent and Briggs (1989). The directional spectral wave basin of 35 m wide by 29 m long has a constant water depth of 0.457 m. The elliptical shoal has a major axis of 3.96 m and minor axis of 3.05 m and a maximum height of 0.3048 m. The shoal boundary is defined by $(X/3.05)^2 + (Y/3.96)^2 = 1$, where X and Y are local coordinates aligned along the minor and major axes, respectively. The wave period T or T_p of the incident waves is 1.3 sec and representative wave height H_{in} or H_s is 2.54 cm. The water depth above the shoal is given as:

$$d(X,Y) = 0.914 - 0.762\sqrt{1-(X/3.81)^2-(Y/4.95)^2} \tag{16}$$

Figure 2 shows a snapshot of the surface elevation for the monochromatic and multi-directional waves cases (H_{in} or H_s =2.54 cm, T or T_p =1.3 sec) . Figure 3 shows a comparison of the model results for narrow directional spectra against the experimental data along the transect No 4 which lies behind the shoal. The comparisons show a good agreement between the model results and the experimental data.

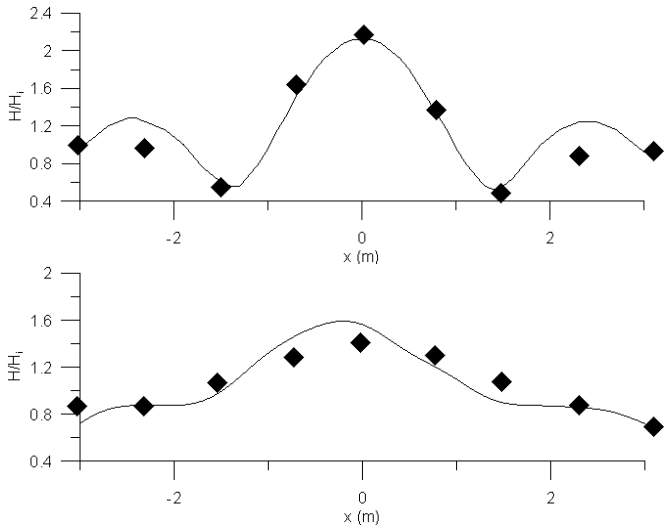

Fig. 3. Comparisons of model results against experimental data of Vincent and Briggs (1989), in terms of normalized wave height H/H_i, for monochromatic (left) and spectral multi-directional waves (right). Numerical model results: solid line, experimental data: symbols.

3.2 Wave diffraction around semi-infinite breakwater

The present numerical solution is compared against the Penney and Price (1944) diffraction solution. Penney and Price (1944) provide an analytical solution for the diffracted wave field about a semi-infinite breakwater based on the Sommerfeld solution of Helmholtz equation using Fresnel integrals for monochromatic waves. The diffraction coefficient $K_D=H/H_i$ is compared with numerical results in Fig. 4. Acceptable agreement is observed between numerical and analytical values.

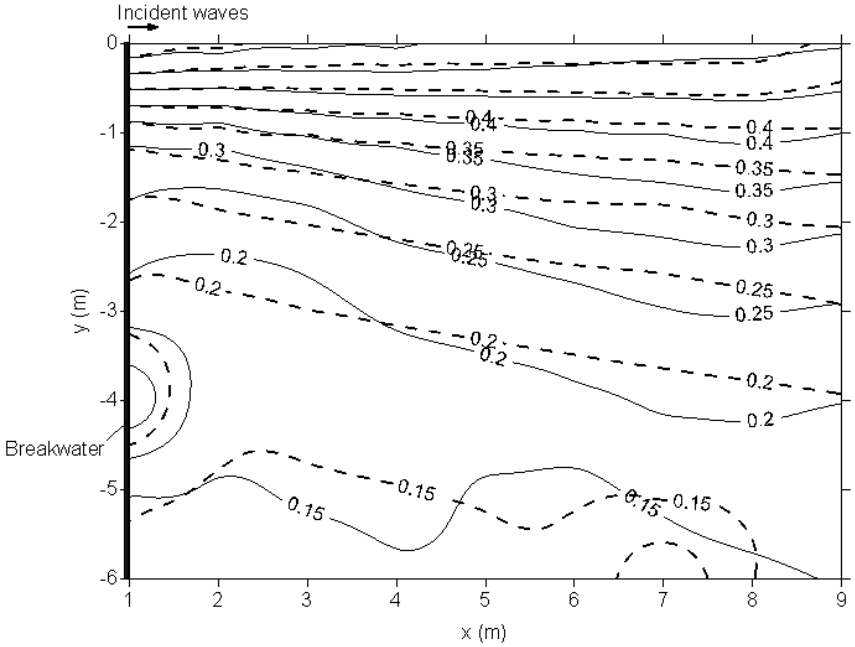

Fig. 4. Wave diffraction behind an infinite breakwater. Comparison of diffraction coefficient $K_D = H/H_i$ (solid line: analytical solution, dashed line: model results).

3.3 Wave diffraction through a breakwater gap

The third set of numerical experiments concern irregular wave diffraction through breakwater gaps (Yu et al., 2000; Li et al., 2000). The incident significant wave height for the case of uni-directional irregular waves is $H_s = 0.05$ m and the peak period is $T_p = 1.20$ s.

Fig. 5 shows the calculated diffraction coefficient for the case of gap width $B = 3.92$ m ($B/L = 2$, where the wave length L corresponds to the peak period for irregular waves). Fig. 6 gives the cross-

section distribution of the diffraction coefficients at a distance $y = 3L$ from the breakwater. Comparisons of model results against experimental data are proven to be satisfactory.

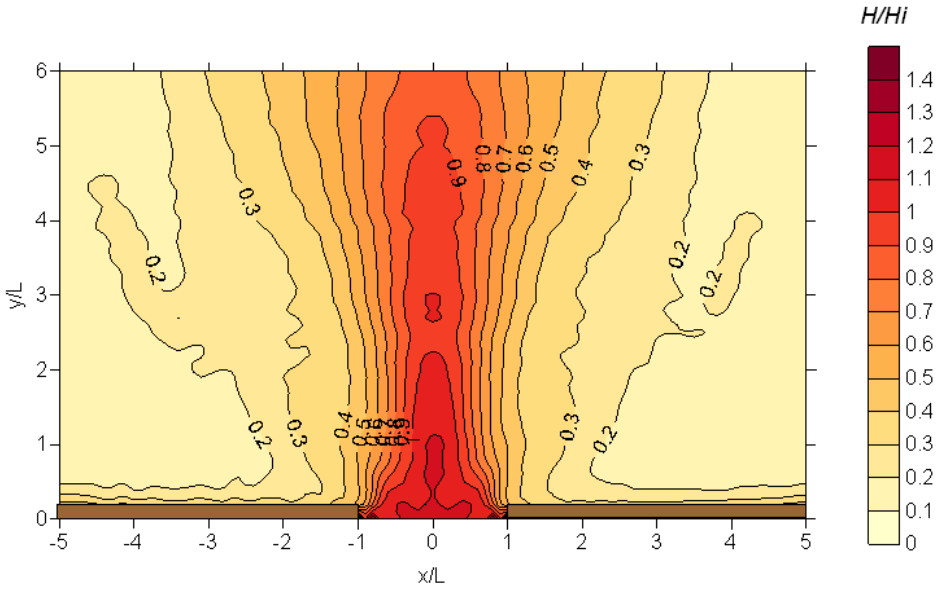

Fig. 5. Wave propagation through breakwater gap: diffraction coefficient contours for B = 3.92 m.

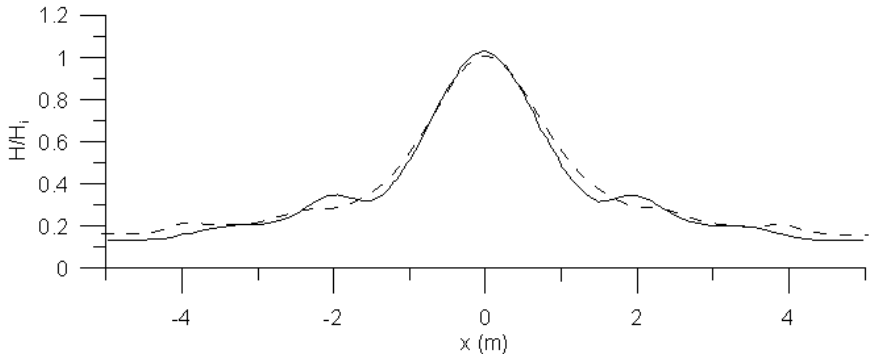

Fig. 6. Wave diffraction behind an infinite breakwater. Comparison of diffraction coefficient $K_D = H/H_i$ at a distance $Y = 3L$ from the breakwater (solid line: experimental data, dashed line: model results).

3.4 Typical model results in realistic bathymetry setups

Fig. 7 presents plotted results concerning simulated fields of gridded data (dx = 2 m) for wave height (top) and free-surface elevation (bottom), in the case of Thessaloniki port (Northern Aegean Sea, Greece). Southwesterly waves with H_s = 1 m and T_p = 8 s, have been reproduced. The unprotected berth areas, as well as the protection offered by the offshore breakwater, are obvious. Partial reflection patterns are also clearly visible.

4 Conclusions

In the present work a new version of a post-Boussinesq nonlinear dispersive wave propagation model has been developed. The model involves only one dispersive term in the momentum equation. The numerical solution is based on a simple explicit Finite Differences scheme and on a numerical evaluation of a convolution integral. The model was successfully applied for wave propagation over varying topographies, behind breakwaters as well as in realistic bathymetry setups. It is concluded that the model is capable to simulate in an accurate and efficient manner the propagation of regular and irregular, nonlinear, dispersive waves over any finite water depth in two horizontal dimensions in the presence of coastal structures. The present model's application is limited only to weakly nonlinear

irregular waves, whereas other Boussinesq-type models (Zou, 1999) can take into account high nonlinearities. In addition, the running time of the model is quite large, and similar to the existing higher order Boussinesq-type models.

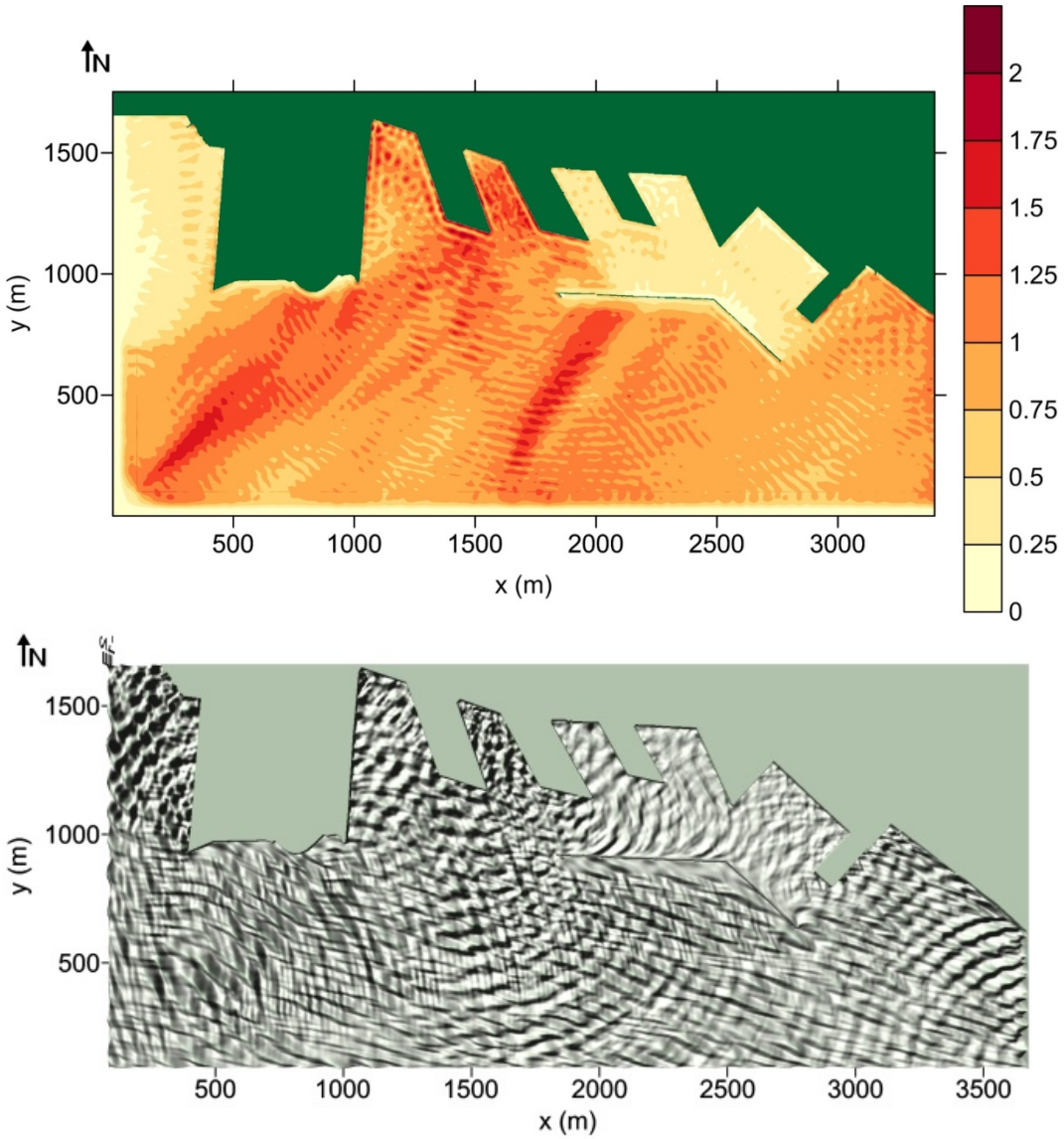

Fig. 7. Multi-directional irregular wave propagation inside the port of Thessaloniki (North Aegean Sea; Greece); Upper graph: wave height (m); Lower graph: free-surface elevation.

Acknowledgements

This research has been co-financed by the European Union and Greek national funds through the Operational Program Competitiveness, Entrepreneurship and Innovation, under the call RESEARCH – CREATE – INNOVATE (Project Name: ACCU-WAVES; Project Code: T1EDK-05111).

References

Berkhoff, J.C.W., Booij, N., Radder, A.C., 1982. Verification of numerical wave propagation models for simple harmonic linear water waves, Coastal Engineering, Elsevier, 6, 255–279.

Bingham, H.B., Agnon, Y., 2005. A Fourier–Boussinesq method for nonlinear water waves, European Journal of Mechanics B/Fluids, 24, 255–274.

Brocchini, M., 2013. A reasoned overview on Boussinesq-type models: the interplay between physics, mathematics and numerics. Proceedings of the Royal Society A: Mathematical, Physical and Engineering Sciences, 469 (2160), 20130496.

Karambas, T., Memos, C., 2009. Boussinesq model for weakly nonlinear fully dispersive water waves, Journal of Waterway, Port, Coastal and Ocean Engineering, ASCE, 135, 187–199.
Karambas, Th.V., Koutitas, C. 2002. Surf and swash zone morphology evolution induced by nonlinear waves, Journal of Waterway, Port, Coastal, and Ocean Engineering, 128 (3), 102-113.
Karambas, Th.V., 1999. A unified model for periodic non linear dispersive wave in intermediate and shallow water. Journal of Coastal Research, 15 (1), 128-139.
Karambas, T.V., Bowers, E.C., 1996. Representation of partial wave reflection and transmission for rubble mound coastal structures, WIT Transactions on Ecology and the Environment**,** 12, 415-423.
Koutitas, C., 1988. Mathematical Models in Coastal Engineering, Pentech Press.
Larsen, J., Dancy, H., 1983. Open boundaries in short wave simulations – a new approach, Coastal Engineering, 7, 285-297.
Lee, C., Suh, K.D., 1998. Internal generation of waves for time-dependent mild-slope equations. Coastal Engineering, 34, 35-57.
Li, Y.S., Liu, S.X., Yu, Y.X., Lai, G.Z., 2000. Numerical modeling of multi-directional irregular waves through breakwaters, Applied Mathematical Modelling, 24 (8-9), 551-574.
Madsen, P.A., Bingham, H.B., Liu, H., 2002. A new Boussinesq method for fully nonlinear waves from shallow to deep water, Journal of Fluid Mechanics, 462, 1-30.
Madsen, P.A., Shäffer, H.A., 1998. Higher-order Boussinesq-type equations for surface gravity waves: derivation and analysis. Phil. Trans. R. Soc. Lond., 356, 3123-3184.
Madsen, P.A., Bingham, H.B., Schäffer, H.A., 2003. Boussinesq type formulations for fully nonlinear and extremely dispersive water waves: derivation and analysis, Proc. R. Soc. Lond., A, 459, 1075–1104.
Miles, M.D., 1989. A note on directional random wave synthesis by the singlesummation method, in: XXIII Congress, IAHR, Canada, C, 243–250.
Nwogu, O., 1993. Alternative form of Boussinesq equations for nearshore wave propagation. Journal of Waterway, Port, Coastal, and Ocean Engineering, 119 (6), 618-638.
Penney, W.G., and Price, A.T. (1944). Diffraction of water waves by breakwaters. Misc. Weapons Development Technical History 26, Artificial Harbors, Sec. 3D.
Peregrine, D.H., 1967. Long waves on a beach, Journal of Fluid Mechanics, 27, 815-827.
Press, W.H., Flanerry, B.P., Teukolsky, S.S., Vetterling, W.T., 1986. *Numerical Recipes*. Cambridge University Press, UK, p. 160-162.
Schäffer, H.A., Madsen, P.A., Deigaard, R., 1993. A Boussinesq model for waves breaking in shallow water, Coastal Engineering, 20, 185-202.
Schäffer, H.A., 2003. Accurate determination of internal kinematics from numerical wave model results, Coastal Engineering, 50, 199-211.
Schäffer, H.A., 2004. Another step twards a post-Boussinesq wave model, in: Proc. of 29th ICCE, ASCE.
Sørensen, O.R., Schäffer, H.A., Madsen P.A., 1998. Surf zone dynamics simulated by a Boussinesq type model. Part III. Wave-induced horizontal nearshore circulations, Coastal Engineering, 33, 155-176.
Tsutsui, S., Suzuyama, K., Ohki, K., 1998. Model equations of nonlinear dispersive waves in shallow water and an application of its simplified version to wave evolution on the step-type reef. Coastal Engineering Journal, 40(1), 41-60.
Vincent, C.L., Briggs, M.J., 1989. Refraction-diffraction of irregular waves over a mound, Journal of Waterway, Port, Coastal and Ocean Engineering, ASCE, 115, 269–284.
Yoon, S. B. and Choi, J. W., 2001. A Note on extension of fully dispersive weakly nonlinear wave equations for rapidly varying topography, Coastal Engineering Journal, 43(3), 143-160.
Wei, G., Kirby, T., 1995. Time-dependent numerical code for extended Boussinesq equations, Journal of Waterway, Port, Coastal, and Ocean Engineering, 121 (5), 251-261.
Wei, G., Kirby, J.T., Grilli, S.T., Subramanya, R., 1995. A fully non-linear Boussinesq model for surface waves: Part I. Highly non-linear unsteady waves, Journal of Fluid Mechanics, 294, 71-92.
Yu, Y.X., Liu, S.X., Li, Y.S., Wai, O.W., 2000. Refraction and diffraction of random waves through breakwater. Ocean Engineering, Elsevier, 27 (5), 489-509.
Zou, Z.L., 1999. Higher order Boussinesq equations, Ocean Engineering, Elsevier, 26, 767-792.